Northumbria Research Link

MME-EKF-Based Path-Tracking Control of Autonomous Vehicles Considering Input Saturation

Chuan Hu, Zhenfeng Wang, Hamid Taghavifar, *Member*, *IEEE*, Jing Na, *Member*, *IEEE*, Yechen Qin*, *Member*, *IEEE*, Jinghua Guo, and Chongfeng Wei

Abstract—This paper investigates the path-tracking control issue for autonomous ground vehicles with the integral sliding mode control (ISMC) considering the transient performance improvement. The path-tracking control is converted into the yaw stabilization problem, where the sideslip-angle compensation is adopted to reduce the steady-state errors, and then the yaw-rate reference is generated for the path-tracking purpose. The lateral velocity and roll angle are estimated with the measurement of the yaw rate and roll rate. Three contributions have been made in this paper: 1) To enhance the estimation accuracy for the vehicle states in the presence of the parametric uncertainties caused by the lateral and roll dynamics, a robust extended Kalman filter is proposed based on the minimum model error algorithm; 2) An improved adaptive radial basis function neural network (RBFNN) considering the approximation error adaptation is developed to compensate for the uncertainties caused by the vertical motion; 3) The RBFNN and composite nonlinear feedback (CNF)-based ISMC is developed to achieve the yaw stabilization and enhance the transient tracking performance considering the input saturation of the front steering angle. The overall stability is proved with Lyapunov function. Finally, the superiority of the developed control strategy is verified by comparing with the traditional CNF with high-fidelity CarSim-Matlab simulations.

Index Terms—Path tracking, autonomous vehicles, sliding mode control, extended Kalman filter, neural network.

I. INTRODUCTION

AUTONOMOUS ground vehicles (AGVs) have attracted large amounts of attention and investment in both the automotive academia and industry over the past decade, due to the gradually increasing demands for the better safety and efficiency in the mobility [1]–[3]. The emergence of AGVs is intended for improving the transportation efficiency, utilization, and most importantly, road security. Rapid advancement in the vehicular cyber-physical system (CPS) and

C. Hu is with the Department of Mechanical Engineering, University of Texas at Austin, Austin, TX 78712, USA.

Z. Wang is with the Automotive Engineering Research Institute, China Automotive Technology and Research Center Co., Ltd., Tianjin, 300300, China.

H. Taghavifar is with the Department of Mechanical and Industrial Engineering, Concordia University, Montreal, QC H3G 1M8, Canada.

J. Na is with Faculty of Mechanical and Electrical Engineering, Kunming University of Science and Technology, Kunming, 650500, China

The corresponding author Y. Qin* is with the School of Mechanical Engineering, Beijing Institute of Technology, Beijing, 100081, China. (e-mail:qinyechenbit@gmail.com)

J. Guo is with the Department of Mechanical and Electrical Engineering, Xiamen University, Xiamen 361005, China.

C. Wei is with the Institute of Transport Studies, University of Leeds, Leeds, LS2 9JT, UK.

especially, the artificial intelligence (AI) technologies [4], [5], have greatly promoted the research and development of AGVs. Challenging driving scenarios and complex traffic environment require AGVs to have higher security, robustness, and efficiency [6], [7]. In this background, it is of great significance and necessity to guarantee high-performance motion control for AGVs from the transient, robust and reliable perspectives [8], [9]. Especially, integrated control combining the yaw and roll dynamics has a great impact on vehicle stability and safety and thus obtains more research focus and effort [10]–[12].

Path tracking is one of the rudimentary motion control objectives of AGVs, which is expected to make the AGV track the desired path given by the path planner in the presence of the unknown disturbances, model uncertainties, and inevitable tire sliding effects [13]. Different path tracking control strategies based on the active front steering (AFS) were developed in various driving scenarios [14]–[16]. However, most of the existing literature about the path tracking control only considered the lateral and yaw dynamics, and generally neglected the roll dynamics. The load transfer or rollover prevention, and their influences on the vertical and lateral dynamics [17], [18] were less been researched previously. Apart from that, the transient performance improvement or input saturation issues had seldom been investigated in the path tracking control design.

Effective path-tracking feedback control highly depends on the accurate acquisitions of vehicle states. Nevertheless, the current literature on the path tracking control generally assumed that the required vehicle states which are hard to measure with low-cost sensors can be measured or obtained. Kalman filters, especially the extended Kalman filter (EKF) and unscented Kalman filter (UKF), have been commonly used for estimating vehicle states or tire forces. Several previous research results were presented by using EKF or UKF for observing the sideslip and roll angles simultaneously [19], [20]. However, traditional Kalman filters heavily rely on precise vehicle models, and generally assume that the model and measurement noise is the white Gaussian noise with the zero mean value and independent mutually. That is a quite rigid assumption for the vehicle system, which is a nonlinear and multi-dimension system in practice. To accelerate the real-time estimation, the vehicle model is usually simplified with limited available model parameters. As a consequence, the simplified model may have time-varying and nonlinear errors that actually cannot be regarded as white Gaussian noise. Such a practice in Kalman filter-based estimators will likely deteriorate the estimation accuracy and then the control

performance.

Consider the above issues, this paper is dedicated to designing a fast, accurate, and robust path tracking control strategy based on the reliable estimation of the vehicle states, considering the system uncertainties caused by the lateral and roll dynamics, input saturation of the front steering angle, and transient performance improvement. A rollover index (load transfer ratio) is adopted in the sliding surface design to enhance the rollover prevention. The underactuation issue for traditional vehicles (i.e., the tires are not independently actuated) is considered in the path-tracking control. To reduce the transient overshoots, oscillations and steady-state errors (SSEs) in the path-tracking control and thus improve the vehicle transient performance and safety, an amendment in the path-tracking kinematics model is adopted based on the sideslip-angle compensation. To summarize, three featured contributions are made: 1) To enhance the estimation precision by eliminating the effects caused by the system uncertainties in the lateral and roll dynamics, the minimum model error (MME) criterion is employed to compensate for the model errors and update the system model for the EKF estimator in real time; 2) To cancel the effects of the nonlinearities and uncertainties, an improved adaptive radial basis function neural network (RBFNN) is developed to approximate the unknown vehicle dynamics, where an adaptation law of the approximation error is developed to improve the estimation accuracy; 3) An integral sliding mode control (ISMC) strategy is developed incorporating the adaptive RBFNN and composite nonlinear feedback (CNF) algorithms to achieve a high-performance yaw control while enhancing the transient performance with the input saturation. The stability is proved with Lyapunov approach.

The rest of this paper is written as follows. The amended path-tracking kinematics, vehicle lateral and roll dynamics modeling is presented in Section II. The MME-based EKF algorithm is developed to estimate the vehicle states in Section III. The observer-based nonlinear ISMC strategy for the path tracking is developed in Section IV. Results of the J-turn high-fidelity simulation with CarSim-Matlab platform are illustrated in Section V. Section VI presents the conclusion.

II. System modelling

A. Amended Modeling of Path-Tracking Kinematics

The amended path-tracking model of AGVs [13] is shown in Fig. 1. e represents the lateral offset from the center of gravity (CG) to the desired path. ψ represents the heading error, i.e., the error between the real heading ψ_h and the reference heading ψ_d, that is, $\psi = \psi_h - \psi_d$. v_x, v_y, β and γ are respectively the longitudinal velocity, lateral velocity, sideslip angle and yaw rate, where $\dot{\psi}_h = \gamma$, and $\beta = \arctan(v_y/v_x) \approx v_y/v_x$ for small sideslip-angle cases. σ refers to the curvilinear abscissa of the point of tangency T from a beginning point. The curvature of the desired path changes with the curvilinear coordinate σ, then is denoted as $\kappa(\sigma)$.

Note that the desired path's tangential direction is usually chosen as the desired heading, which however may deteriorate the path tracking performance, especially when the vehicle
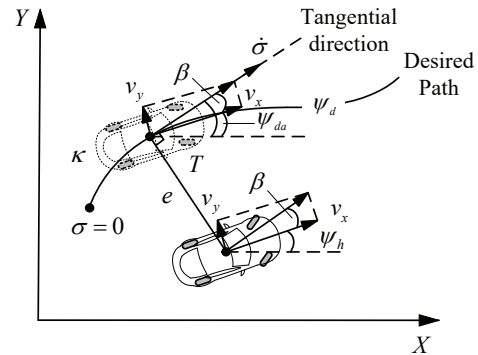

Fig. 1. Amended path-tracking kinematics model

is making a sharp turning. The reason for this can be interpreted as: the lateral control and yaw control are actually conflicting in the presence of tire sliding effects for traditional vehicles, and the lateral speed is not zero if the vehicle makes turnings. By adopting a modification to the desired-heading definition, the SSEs of the path-tracking errors can be considerably reduced [13]. Therefore this amendment is adopted here to promote the transient response of the path tracking. Based on Fig. 1, the new desired-heading ψ_{da} is defined as $\psi_{da} = \psi_d - \beta$. So the amended heading error is defined as $\psi = \psi_h - \psi_{da} = \psi_h - \psi_d + \beta$. Then the amended path-tracking kinematics model for AGVs can be described as

$$\begin{aligned} \dot{e} &= v_x \sin \psi + v_y \cos \psi, \\ \dot{\psi} &= \gamma - \kappa(\sigma) v_x + \dot{\beta}. \end{aligned} \tag{1}$$

The yaw-rate reference for the path tracking purpose developed in [13], [21] has a simplified form but achieves a satisfactory tracking performance, thus is adopted as

$$r = \kappa(\sigma) v_x - \ell_2 (\psi + \ell_1 e) - \dot{\beta}, \tag{2}$$

where ℓ_1 and ℓ_2 are positive constants chosen to satisfy that $\ell_1 = 1/L$, $\ell_2 > v_x/L$, where L is the lookahead distance [22]. In the Section III the vehicle states including β will be estimated with an EKF, then $\dot{\beta}$ can be reliably obtained by several effective observers or differentiators [23].

The control objective in path-tracking control generally refers to making the vehicle maintain in the desired lane, and follow the predefined path asymptotically, that is, to design an appropriate control strategy to globally and asymptotically stabilize the path tracking errors to zero.

B. Modeling of Vehicle Lateral and Vertical Dynamics

A 2 DoF "bicycle" vehicle model is formulated to describe the vehicle lateral and yaw dynamics as shown in Fig. 2. I_z and m represent the yaw inertia moment and the total vehicle mass, respectively. l_f and l_r represent the front and rear axle distance from the CG respectively. F_{yf} and F_{yr} stand for the integrated lateral forces of the front and rear tires, respectively. δ_f is the steering angle of the front wheel. As the vehicle longitudinal dynamics can be independently controlled, here it is assumed that the longitudinal velocity v_x is a constant. Assume the tire slip angles and steering angle are sufficiently
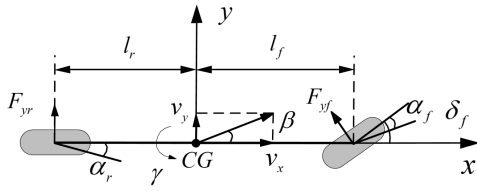
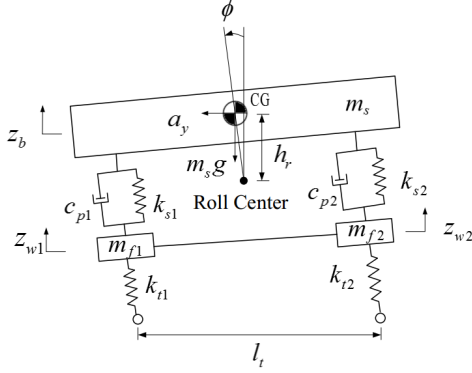Fig. 2.   2 DoF "bicycle" vehicle model with sliding effects.

Fig. 3.   Half-car roll dynamics model.

small, so the tires work in the linear region, and the vehicle yaw and lateral dynamics can be modeled as

$$\dot{\gamma} = \frac{(-l_f{}^2 c_f - l_r{}^2 c_r)}{v_x I_z}\gamma + \frac{(l_r c_r - l_f c_f)}{I_z v_x}v_y + \frac{l_f c_f}{I_z}\delta_f,$$

$$\dot{v}_y = \left(-v_x - \frac{l_f c_f - l_r c_r}{m v_x}\right)\gamma - \frac{(c_f + c_r)}{m v_x}v_y + \frac{c_f}{m}\delta_f, \quad (3)$$

where c_f and c_r represent the integrated front and rear cornering stiffnesses.

A 4 DoF half-car model is developed for the vehicle roll dynamics as shown in Fig. 3 [24]. m_s represents the vehicle sprung mass. k_{s1} and k_{s2} represents the left and right-side suspension stiffness (it is assumed $k_s = k_{s1} = k_{s2}$), c_{p1} and c_{p2} represents the left and right suspension damping coefficient (it is assumed $c_p = c_{p1} = c_{p2}$), m_{f1} and m_{f2} are the left and right unsprung mass of the vehicle (it is assumed $m_f = m_{f1} = m_{f2}$), and k_{t1} and k_{t2} are the left and right tire stiffnesses (it is assumed $k_t = k_{t1} = k_{t2}$), respectively. z_b, z_{w1} and z_{w2} represent the vertical translations of the sprung mass, left and right unsprung masses, respectively. f_1 and f_2 are the active force at the front and rear active suspensions, respectively. ϕ represents the roll angle of the sprung mass. The roll dynamics can be formulated as

$$(I_x + m_s h_r^2)\ddot{\phi} = m_s h_r\left(a_y \cos\phi + g\sin\phi\right) - \frac{l_t}{2}(F_{s1} - F_{s2}), \quad (4)$$

where I_x is the longitudinal inertia moment, h_r is the distance between the sprung mass CG and the roll center. l_t is the track width. a_y is the lateral acceleration. F_{s1} and F_{s2} represent the left and right suspension forces, respectively, which can be

expressed as

$$F_{s1} = -k_{s1}(z_b - z_{w1} - \frac{l_t \sin\phi}{2}) - c_{p1}(\dot{z}_b - \dot{z}_{w1} - \frac{l_t\dot{\phi}\cos\phi}{2}),$$

$$F_{s2} = -k_{s2}(z_b - z_{w2} + \frac{l_t \sin\phi}{2}) - c_{p2}(\dot{z}_b - \dot{z}_{w2} + \frac{l_t\dot{\phi}\cos\phi}{2}). \quad (5)$$

To evaluate the roll behavior of the vehicle, the load transfer ratio (LTR) is defined based on the difference of the vertical forces between the left and right tires as follows

$$LTR = \frac{F_{zr} - F_{zl}}{F_{zr} + F_{zl}} = \frac{2m_s}{m l_t}\left[(h_r + h\cos\phi)\frac{a_{ys}}{g} + h\sin\phi\right], \quad (6)$$

where F_{zl} and F_{zr} represent the vertical forces on the left and right tires, respectively. h is the height of the vehicle CG. $a_{ys} = a_y - h\ddot{\phi}$ is the lateral acceleration of the unsprung mass. The vehicle roll dynamics is stable when the LTR equals to 0, the rollover risk becomes greater when LTR goes toward ± 1, and the wheel will lift off when LTR equals to ± 1.

III. STATE ESTIMATION

In this section, an EKF based on the MME criterion is developed to estimate the lateral velocity and roll angle, which are generally hard to measure. In the estimation, it is assumed the measurements of the yaw rate and roll rate are available.

A. Problem Formulation for Estimation

According to the vehicle dynamics in (3) and (4), this paper defines $x = [v_y, \gamma, \phi, \dot{\phi}]^T$, $y = [\gamma, \dot{\phi}]^T$ and $u = \delta_f$ as the observer state, measured output, and input, respectively. Substituting (3), (5) and the lateral acceleration which can be expresses as $a_y = \dot{v}_y + v_x\gamma$ into (4), we have

$$(I_x + m_s h_r^2)\ddot{\phi} = \frac{m_s h_r(l_r c_r - l_f c_f)}{m v_x}\gamma + \left(m_s h_r g - \frac{l_t^2}{2}k_s\right)\phi$$
$$- \frac{l_t^2}{2}c_p\dot{\phi} + m_s h_r\frac{c_f}{m}\delta_f - m_s h_r\frac{(c_f + c_r)}{m v_x}v_y$$
$$+ \frac{l_t k_s}{2}(z_{w2} - z_{w1}) + \frac{l_t c_p}{2}(\dot{z}_{w2} - \dot{z}_{w1}). \quad (7)$$

Since the dynamics of the coupled vehicle systems are highly affected by the lateral tire force [25], this paper develops an EKF based on the MME criterion, which takes the uncertainty of the lateral tire forces F_{yi} ($i = f, r$) into consideration to improve the estimation accuracy. The uncertainties contained in F_{yi} is formulated as $F_{yi} = \bar{F}_{yi} + \Delta F_{yi} + w_i$, where $\bar{F}_{yi}$ and ΔF_{yi} are the nominal later tire force and its uncertainty, respectively, and w_i is the measurement noise. Considering the model errors and uncertainties, the state dynamics can be expressed as

$$\dot{x} = f(x, u) + E_s, \quad (8)$$

where $f(x, u) = [f_1, f_2, \dot{\phi}, f_4]^T$ with

$$f_1 = -\frac{(c_f + c_r)}{m v_x}x_1 + \left(-v_x - \frac{l_f c_f - l_r c_r}{m v_x}\right)x_2 + \frac{c_f}{m}u,$$

$$f_2 = \frac{(l_r c_r - l_f c_f)}{I_z v_x}x_1 + \frac{(-l_f^2 c_f - l_r^2 c_r)}{v_x I_z}x_2 + \frac{l_f c_f}{I_z}u,$$

$$f_4 = \frac{1}{(I_x + m_s h_r^2)} \left[\frac{-m_s h_r (c_f + c_r)}{m v_x} x_1 + \frac{m_s h_r (l_r c_r - l_f c_f)}{m v_x} x_2 \right.$$

$$+ \left(m_s h_r g - \frac{l_t^2}{2} k_s \right) x_3 - \frac{c_p l_t^2}{2} x_4 + \frac{m_s h_r c_f}{m} u$$

$$\left. + \frac{l_t k_s}{2} (z_{w2} - z_{w1}) + \frac{l_t c_p}{2} (\dot{z}_{w2} - \dot{z}_{w1}) \right],$$

and $E_s = [\varepsilon_{s,1}, \ \varepsilon_{s,2}, \ \varepsilon_{s,3}, \ \varepsilon_{s,4}]^T$ represents the unmodeled system uncertainties and disturbance including the effects caused by the tire force uncertainties and measurement noise. E_s can be described as

$$E_s = G\Lambda + w, \tag{9}$$

where $\Lambda = [\Delta F_{yf}, \Delta F_{yr}]^T$ is the uncertainties of the lateral tire forces, $w = [w_1, \ w_2, \ w_3, \ w_4]^T$ represents the measurement noise vector. Note that we have verified the proposed estimation strategy in CarSim platform, where the noise and drift issues of the measurements of the yaw rate and roll rate are in reasonably small regions, and thus have limited effects on the estimation performance. Also, the proposed estimator, MME-EKF and the controller, ISMC have good robustness to deal with the sensor drift and noise. Denote $Q = \text{diag} \left(\sigma_{w,1}^2, \sigma_{w,2}^2, \sigma_{w,3}^2, \sigma_{w,4}^2 \right)$ as the covariance of the process noise, where $\sigma_{w,i}^2$ is the variance of ith element, and G is the error propagation matrix. From (3) and (4), G can be calculated as

$$G = \begin{bmatrix} 1/m & -(l_f + 1)/I_z v_x & 0 & g_4 \\ 1/m & -(l_r - 1)/I_z v_x & 0 & g_4 \end{bmatrix}^T, \tag{10}$$

where $g_4 = m_b h_{roll}/m \left(I_x + m_b h_{roll}^2 \right)$.

Considering the noise, the measured output can be modeled as $y = h(x) + v$, where $h(x) = [x_2, x_4]^T$. Based on the discussion above, the state-space form of the system can be formulated as follows

$$\begin{aligned} \dot{x} &= f(x, u) + G\Lambda + w, \\ y &= h(x) + v, \end{aligned} \tag{11}$$

where v is the measurement noise with the covariance matrix of $R = \text{diag} \left(\sigma_{v,1}^2, \sigma_{v,2}^2 \right)$. The discrete-time expression of the state-space representation can be expressed as

$$\begin{aligned} x(k) &= x(k-1) + Tf(x(k-1), u(k-1)) \\ &\quad + TG(k-1)\Lambda(k) + Tw(k-1), \end{aligned} \tag{12}$$

$$y(k) = h(x(k)) + v(k), \tag{13}$$

where T is the sample time. The main purpose of MME criterion is to improve the observation accuracy by considering the system uncertainties.

B. Error Compensation with MME Criterion

The main procedure of MME can be illustrated as: Firstly the compensator calculates the error Λ based on the system inputs and measurements. The compensation is then used to improve the modeling accuracy. EKF finally adopts the compensated system model to estimate system states under random process and measurement noise. The objective function of the MME compensator is expressed as [26], [27]

$$J[\Lambda(k)] = \frac{1}{2} \tilde{y}(k)^T R^{-1} \tilde{y}(k) + \frac{1}{2} \Lambda^T(k) \Gamma \Lambda(k), \tag{14}$$

where $\tilde{y}(k) = y(k) - \hat{y}(k)$, Γ is the weight matrix of $\Lambda(k)$, and $\hat{y}(k)$ is the output estimation at the current step $\hat{y}(k) = h(\hat{x}(k|k))$, where $\hat{x}(k|k)$ is the predicted system state at $k-1$ step. By combining (13) and $\hat{y}(k)$ we have

$$\begin{cases} \hat{y}(k) = h(\hat{x}(k-1|k-1)) + T\frac{\partial h}{\partial x} \dot{x}|_{x=\hat{x}(k-1|k-1)}, \\ T\frac{\partial h}{\partial x} \dot{x} = TL_G(h)\Lambda(k) + TL_f(h), \end{cases} \tag{15}$$

where $\partial h/\partial x$ represents the Jacobi matrix of the output equation, $L_G(h)$ and $L_f(h)$ are the first-order Lie derivations of h_x w.r.t. G and $f(x, u)$, which can be expressed as

$$\begin{cases} TL_G(h) = \frac{\partial h(x)}{\partial x} G|_{\hat{x} = \hat{x}(k-1|k-1)}, \\ TL_f(h) = \frac{\partial h(x)}{\partial x} f(x, u)|_{\hat{x} = \hat{x}(k-1|k-1)}. \end{cases} \tag{16}$$

The optimal lateral tire force uncertainty Λ can then be calculated based on the minimum value principle as

$$\begin{cases} \Lambda(k) = -\left[\Theta(k)^T R^{-1} \Theta(k) + \Gamma \right]^{-1} \cdot \\ \qquad \Theta(k)^T R^{-1} [S(k) + \hat{y}(k) - y(k)], \\ \hat{y}(k) = h(\hat{x}(k-1|k-1)), \end{cases} \tag{17}$$

where $\Theta(k) = TL_G(h)$ and $S(k) = TL_f(h)$. One critical parameter of the MME algorithm is the weight matrix Γ, which should be chosen to make the observation equation (17) satisfy the following equality constraint for the covariance

$$\frac{1}{Z} \sum_{z=1}^{Z} \{ y(z) - \hat{y}(z) \} \{ y(z) - \hat{y}(z) \}^T \approx R, \tag{18}$$

where Z is the time scale for approaching R.

C. Estimation via EKF Based on the MME Criterion

This part formulates the estimator with MME-EKF based on the developed error compensator. The process and measurement matrixes are firstly initialized, and the lateral tire force uncertainty Λ is then calculated and provided to the EKF module to improve the estimation accuracy. Based on the above analysis, the discrete form of MME-EKF for the investigated system can be summarized as

$$\begin{aligned} x(k|k-1) &= Tf(x(k-1|k-1), u(k-1)) \\ &\quad + x(k-1|k-1) + TG(k-1)\Lambda(k), \\ y(k|k-1) &= h(x(k|k-1)), \\ P(k|k-1) &= A'(k) P(k-1|k-1) A'(k)^T + T^2 Q, \\ K(k) &= P(k|k-1) C'^T(k) \cdot \\ &\quad \left[C'(k) P(k|k-1) C'(k)^T + R \right]^{-1}, \\ x(k|k) &= x(k|k-1) + K(k) [y(k) - y(k|k-1)], \\ P(k|k) &= [I - K(k) C'(k)] P(k|k-1), \end{aligned} \tag{19}$$

where $x\left(k-1|k-1\right)$ and $P\left(k-1|k-1\right)$ are the optimal estimated state and error covariance matrix at $k-1$ step, respectively. $K\left(k\right)$ is the feedback matrix gain of Kalman filter, and I is an unit matrix. Both A' and C' are the Jacobian matrixes derived according to the system dynamics, which can be expressed as

$$A'\left(k\right) = T\frac{\partial f\left(x\left(k\right), u\left(k\right)\right)}{\partial x\left(k\right)} + I,$$

$$C'\left(k\right) = \frac{\partial h\left(x\left(k\right)\right)}{\partial x\left(k\right)}. \tag{20}$$

Combining the current input, measurements, and estimations of the last step, as well as the statistical information of the system and measurement noise, the EKF can update the current estimation gain, covariance matrices of the system states and errors according to (19).

IV. Observer-based ISMC Controller Design

In this section, an improved ISMC is designed to make the yaw rate track its reference value considering the state immeasurabilities, input saturation, transient performance, and system uncertainties, where the desired yaw rate is generated according to the path-following objective. A system diagram is shown in Fig. 4 to present the overall depiction of the path following control. There are two reasons to use ISMC instead of traditional SMC: 1) ISMC can make the closed-loop system have the complete robustness or insensitivity in the whole response from the initial time instance to the reaching mode; 2) ISMC is more flexible in term of the controller structure, as it consists of a nominal controller to achieve specific control objective and an additional SMC controller to cancel the effects of the disturbances or uncertainties. However, traditional SMC doesn't have those two features. In this sense, we can use ISMC to incorporate a CNF controller to improve the transient control performance. As for the justification, we have used the traditional CNF as the controller benchmark for the comparative simulations to justify the advantages of ISMC method, the readers can also refer to our previous papers on ISMC [7], [28] and theoretical literature on ISMC [29], [30].

Denote $\xi = [\gamma, \quad \phi, \quad \dot{\phi}]^{\mathrm{T}}$ and $u = \delta_f$ as the system state and control input, respectively. Based on the modeling presented in Section II, the control-oriented vehicle model for the path-tracking purpose can be written as

$$\dot{\xi} = A\xi + Bu + E\bar{d}, \tag{21}$$

where

$$A = \begin{bmatrix} a_{11} & 0 & 0 \\ 0 & 0 & 1 \\ a_{31} & a_{32} & a_{33} \end{bmatrix}, B = \begin{bmatrix} b_1 \\ 0 \\ b_3 \end{bmatrix}^T, E = \begin{bmatrix} e_{11} & 0 & 0 \\ 0 & 0 & 0 \\ e_{31} & e_{32} & e_{33} \end{bmatrix},$$

with

$$a_{11} = \frac{-l_f^2 c_f - l_r^2 c_r}{v_x I_z}, a_{31} = \frac{m_s h_r (l_r c_r - l_f c_f)}{(I_x + m_s h_r^2) m v_x}, a_{32} = \frac{2 m_s h_r g - l_t^2 k_s}{2(I_x + m_s h_r^2)},$$

$$a_{33} = \frac{-l_t^2 c_p}{2(I_x + m_s h_r^2)}, b_1 = \frac{l_f c_f}{I_z}, b_3 = \frac{m_s h_r c_f}{m(I_x + m_s h_r^2)}, e_{11} = \frac{l_r c_r - l_f c_f}{I_z v_x},$$

$$e_{31} = -\frac{m_s h_r (c_f + c_r)}{m v_x (I_x + m_s h_r^2)}, e_{32} = \frac{l_t k_s}{2(I_x + m_s h_r^2)}, e_{33} = \frac{l_t c_p}{2(I_x + m_s h_r^2)},$$

and $\bar{d} = [\begin{array}{ccc} v_y & z_{w2} - z_{w1} & \dot{z}_{w2} - \dot{z}_{w1} \end{array}]^T$ is regarded as the unknown disturbance, as its elements can be assumed to be sufficiently small. Note that in this work, we have used the CNF algorithm to constrain the steering angle in a small and reasonable region, thus it is reasonable to assume the v_y is sufficiently small. Considering the saturation issue of the steering angle and facilitating the controller design for ISMC, (21) is organized into the following form

$$\dot{\xi} = A\xi + B\left[\mathrm{sat}\left(u\right) + d\right],$$
$$y = C_1 \xi, \ z = C_2 \xi, \tag{22}$$

where $\mathrm{sat}\left(u\right) = \mathrm{sign}\left(u\right) \cdot \min\{u_{\max}, |u|\}$ with $u_{\max} = \delta_{f\max}$ being the saturation limit for the steering wheel angle. $d = \left(B^T B\right)^{-1} B^T E\bar{d}$ is transformed as a lumped disturbance, which can be identified to be a scalar. $y = [\begin{array}{cc} \gamma & \dot{\phi} \end{array}]^T$ is the measurable output. $z = \gamma$ is the regulated output. r is the yaw-rate reference for the regulated output z given in (2) based on the path-tracking objective. As it is assumed v_x is a constant, so there is no singularity problem in the modeled system. The matrixes of C_1 and C_2 can be written as

$$C_1 = \begin{bmatrix} 1 & 0 & 0 \\ 0 & 0 & 1 \end{bmatrix}, C_2 = \begin{bmatrix} 1 & 0 & 0 \end{bmatrix}. \tag{23}$$

The desire of the ISMC control is to make the system trajectory to stabilize on the sliding surface at $s\left(\xi, t\right) = 0$. The ISMC controller u is developed as $u = u_0 + u_s$, where u_0 is the nominal controller to realize the desired performance when the overall system is not disturbed, which will be designed later based on CNF algorithm to enhance the transient tracking performance in this work. u_s is the additional SMC controller to compensate for the external disturbances.

Remark 1: Note that we have regarded the v_x as a constant in this work, as v_x can be independently controlled, while in this work the main contribution in the control part is that we have proposed a CNF-based ISMC to improve the transient performance, by integrating an improved adaptive RBFNN. Therefore we have focused on the control algorithm side, used a 2 DoF vehicle model and assumed the v_x is a constant, which can facilitate the controller design. Actually we have focused on the dangerous manoeuvers (including the J-turn on the slippery road with low speed, and the lane change on the dry road with high speed), thus within those respective manoeuvers the vehicle longitudinal speed can be assumed as a constant in those short periods. As for the small values of the tire slip angles and the front steering angle, since we have considered the dangerous driving scenarios, we have constrained the front steering angle within a small region, thus the tire slip angles will be reasonably small, which can be found in the later simulation results.

To achieve the path-tracking control with the rollover prevention and constrained input, an improved integral sliding surface is defined as

$$s\left(\xi, t\right) = G_s\left\{\xi\left(t\right) - \xi\left(0\right) - \int_0^t \left(A\xi + B\Delta\right) d\tau\right\}, \tag{24}$$

where $G_s = [g_{s1}, \vartheta_1\left(LTR\right), g_{s3}]$ with g_{s1} and g_{s3} being two constants to be designed, and $\vartheta_1\left(LTR\right)$ being an adap-

tion gain with a nonlinear barrier function form. Note that generally in ISMC framework, $G_s B$ should be designed as an uniformly invertible matrix, and it turns into a scalar in this work. $\vartheta_1 (LTR)$ is designed to be time-varying according to the vehicle roll dynamics behaviour as $\vartheta_1 (LTR) = (1/80) \ln \sigma_{\max}^2 / (\sigma_{\max}^2 - LTR^2) + 1$, which is a smooth, nonlinear and nondecreasing barrier function with respect to the LTR defined in (6). $\vartheta_1 (LTR)$ is used to adaptively change the weight of the roll angle control in the sliding surface. $\sigma_{\max}$ is a conservative safe boundary to prevent vehicle rollover, which can be chosen as 0.6 [31]. Δ represents the constrained nominal control portion considering the input saturation defined as $\Delta = \text{sat}(u) - u_s$.

The common choice for the additional SMC controller u_s is given by $u_s = -M\text{sign}[(G_s B)^T s(\xi, t)]$, where M is a positive constant satisfying $M \geq d_m$, with d_m being the bound of $||d||$. Without the loss of generality we can consider $G_s B = I_{1\times1}$. The time derivative of s can be given from (24) as $\dot{s} = G_s B(u_s + d)$. Such a controller's actual control effect is equivalent to that of an "equivalent controller". For the purpose of the analysis for the overall stability, u_s can be changed with its equivalent controller $(u_s)_{eq} = u_{seq} = -d$.

Remark 2: Disturbance observer-based SMC is also an applicable method for the robust control with matched and mismatched uncertainties [32], [33], which can achieve good performance and robustness. We used the neural network to approximate the disturbances for the following reasons: 1) The neural network approach doesn't need an exact mathematical model and thus has been widely used in the estimation of nonlinear systems [34], [35]. In this work, we used a high-fidelity and full-car model with CarSim software to implement the simulation, it would be more accurate to estimate the disturbances or uncertainties using the neural network, a data-oriented approach than using a model-based estimation method, since the vehicle system model is nonlinear and complex; 2) The neural network system has capability of approximating any nonlinear function with arbitrary precision on a compact set based on the universal approximation theorem [36], thus it can achieve very accurate estimation based on a large amount of training data.

A. Nominal Controller Design Using CNF

Path-tracking performance for AGVs heavily relies on the effective steering actuation. In this subsection, we will develop a nominal controller with CNF strategy for the system free from disturbances to generate a desired path with the time-varying target reference and input constraint, and enhance the transient performance, including reducing the oscillations and eliminating the SSEs.

Firstly, a linear feedback controller u_l for the system (22) with the time-varying reference is developed as

$$u_l = F\xi + G_c r + G_r \dot{r}, \qquad (25)$$

where F is the feedback control gain, and should satisfy that 1) $A + BF$ is an asymptotically stable matrix; 2) the dominant pair of the closed-loop poles of $C_2(s^\dagger I - A - BF)^{-1}B$ ($s^\dagger$ represents the Laplace variable) is designed to have a small

damping ratio, which would then in turn generate a quick rise time for the system response. G_c and G_r are developed to realize the feedforward control respectively chosen as $G_c = -[C_2(A + BF)^{-1}B]^{-1}$, and G_r is chosen as $G_r = B^T (BB^T)^{-1} \bar{G}$, where $\bar{G} = -(A + BF)^{-1}BG_c$, where the linear feedback part is developed to force the control output z to track the reference r.

Secondly, given any symmetric positive definite matrix $W_c \in \mathbb{R}^{3\times3}$, by solving the following Lyapunov equation, we can obtain a symmetric positive definite matrix $P_c \in \mathbb{R}^{3\times3}$

$$(A + BF)^T P_c + P_c (A + BF) = -W_c. \qquad (26)$$

We denote $\bar{\xi}$ as the reference of the system state ξ and ξ_e as the error between ξ and $\bar{\xi}$ as $\bar{\xi} = \bar{G}r$ and $\xi_e = \xi - \bar{\xi}$, implying that ξ will track $\bar{\xi}$ as z tracks r. The nonlinear feedback u_n is developed as

$$u_n = \rho(r, z) B^T P_c (\xi - \bar{\xi}), \qquad (27)$$

where $\rho(r, z)$ is a non-positive and smooth function of $||z - r||$ used to change the damping ratio adaptively to yield a higher transient performance. A scaled nonlinear function [37] is adopted in this study, since it had been proved to have better robustness to the variation of the tracking reference.

Lastly the two feedback control portions are integrated $(u_0 = u_l + u_n)$ to construct the final CNF controller as

$$u_0 = F\xi + G_c r + G_r \dot{r} + \rho(r, z) B^T P_c \cdot (\xi - \bar{\xi}). \qquad (28)$$

B. Additional SMC Controller Design Using Adaptive RBFNN

An additional SMC controller is developed to remove the effects of the external disturbance and thus to make the path-tracking controller robust, where the disturbance is compensated with the RBFNN approach.

As a classic feedforward NN, the RBFNN has been widely applied in various applications due to its advantages of fast training capability, simple structure and capability of convergence to global optimization [38], [39]. Given any continuous function $Z(x)$ defined over the compact set, there exists a NN function $W^T \varphi(x)$ to approximate $Z(x)$ with arbitrary accuracy as $Z(x) = W^T \varphi(x) + \varepsilon$, where $W = [\omega_1, \omega_2, \cdots \omega_N]^T$ is the adjustable weighting vector, and $\varphi(x) = [\varphi_1(x), \varphi_2(x), \cdots \varphi_N(x)]^T$ is the radial basis vector with N being the number of neurons, and ε is the approximation error. $\varphi_i(x)$ is selected as a Gaussian function

$$\varphi_i(\xi) = \exp\left(-||x - C_i||^2 / \sigma_i^2\right), \quad i = 1, \ 2, \ \cdots, N, \quad (29)$$

where $C_i = [c_{i1}, \ c_{i2}, \ \cdots, c_{iN}]^T$ is the center of the receptive field, σ_i is the width of the Gaussian function. In this paper an adaptive RBFNN is developed to approximate the lumped disturbance $(G_s B) d$ which can be regarded as the output of the RBFNN as $(G_s B) d = W^T \varphi(s) + \varepsilon$, where W is the optimal weights matrix, and s is chosen as the input of the network. Based on the above analysis, a SMC controller based on the adaptive RBFNN algorithm is developed as:

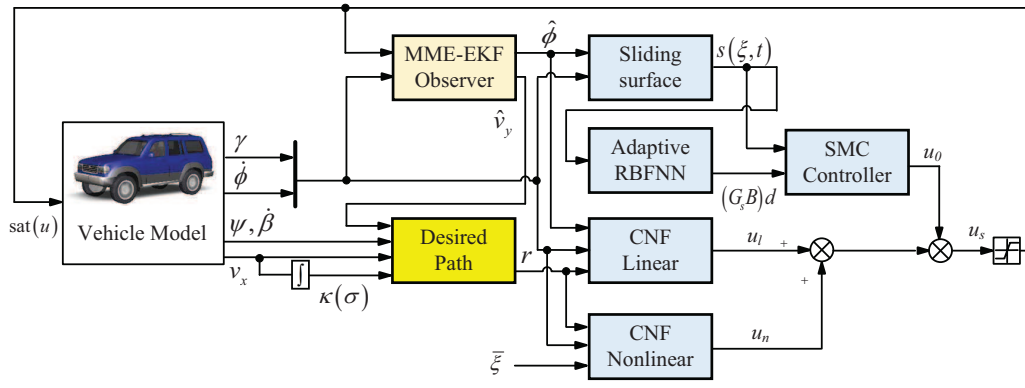*Theorem 1*: For the given system with unknown disturbance,

Fig. 4.   Schematic diagram of the proposed path-following control.

with the following controller

$$u_s = (G_s B)^{-1} \left[-k_1 s - k_2 \text{sign}(s) - \hat{W}^T \varphi - \hat{\varepsilon} \right], \quad (30)$$

where $\hat{W}$ and $\hat{\varepsilon}$ are respectively the estimations of weight matrix W^* and approximation error ε, which are designed as

$$\dot{\hat{W}} = \Gamma_s \left(S\varphi - \sigma_w \hat{W} \right),$$
$$\dot{\hat{\varepsilon}} = -\sigma_\varepsilon \eta \hat{\varepsilon} \quad (31)$$

where $S = \text{diag}\{s_1, \cdots, s_N\}$ with $s = [s_1, \cdots, s_N]^T$, the sliding variable s and $\dot{s}$ can be driven to zero asymptotically and globally in finite time. Note that $N = 1$, we present S and s in the vector/matrix form in the following proof to present the integrated approach for the condition of $N > 1$. σ_w, σ_ε, and η are positive constants, and Γ_s is the symmetrical positive definite matrix, which is related to the adaption rate.

Remark 3: Note that there are several advanced adaptation laws for $\hat{W}$, such as concurrent-learning algorithm [40], [41], which has many performance benefits, including exponential stability and convergence. Nevertheless, our research focus and the main feature of the control strategy design are to improve the transient tracking performance in the transient period, and the investigated system in this work, path-tracking control of autonomous vehicles with the changing road curvatures, can generally satisfy the requirement of persistency of excitation. Moreover, the used adaptive RBFNN has achieved good enough estimation accuracy in the high-fidelity simulations later, and have more concise expression and lower computation loads, so we have used the traditional RBFNN approach to approximate the lumped disturbance.

Proof: Design the Lyapunov function as

$$V_2 = \frac{1}{2} s^T s + \frac{1}{2} \tilde{W}^T \Gamma_s^{-1} \tilde{W} + \frac{1}{2\eta} \tilde{\varepsilon}^T \tilde{\varepsilon}, \quad (32)$$

whose time derivative is given by

$$\dot{V}_2 = s^T \dot{s} + \tilde{W}^T \Gamma_s^{-1} \dot{\tilde{W}} + \frac{1}{\eta} \tilde{\varepsilon}^T \dot{\tilde{\varepsilon}}$$
$$= s^T \left[(G_s B) u_s + (G_s B) d \right] + \tilde{W}^T \Gamma_s^{-1} \dot{\tilde{W}} + \frac{1}{\eta} \tilde{\varepsilon}^T \dot{\tilde{\varepsilon}}$$
$$= s^T \left[-k_1 s - k_2 \text{sign}(s) - \hat{W}^T \varphi - \hat{\varepsilon} + (G_s B) d \right] \quad (33)$$
$$+ \tilde{W}^T \Gamma_s^{-1} \dot{\tilde{W}} + \eta^{-1} \tilde{\varepsilon}^T \dot{\tilde{\varepsilon}}.$$

With $\tilde{W} = W - \hat{W}$ and $\tilde{\varepsilon} = \varepsilon - \hat{\varepsilon}$, we have $\dot{\tilde{W}} = -\dot{\hat{W}}$ and $\dot{\tilde{\varepsilon}} = -\dot{\hat{\varepsilon}}$. Considering the following equations $\tilde{W}^T \hat{W} \le -0.5\|\tilde{W}\|^2 + 0.5\|W\|^2$, $\tilde{\varepsilon}\hat{\varepsilon} \le -0.5\|\tilde{\varepsilon}\|^2 + 0.5\|\varepsilon\|^2$, (33) can be rewritten as

$$\dot{V}_2 = s^T \left[-k_1 s - k_2 \text{sign}(s) - \hat{W}^T \varphi - \hat{\varepsilon} + W^T \varphi + \varepsilon \right]$$
$$\quad - \tilde{W}^T \Gamma_s^{-1} \left[\Gamma_s \left(S\varphi - \sigma_w \hat{W} \right) \right] + \eta^{-1} \tilde{\varepsilon}^T \sigma_\varepsilon \eta \hat{\varepsilon}$$
$$= -k_1 s^T s - k_2 s^T \text{sign}(s) + s^T \tilde{W}^T \varphi + s^T \tilde{\varepsilon}$$
$$\quad - \tilde{W}^T S\varphi + \sigma_w \tilde{W}^T \hat{W} + \sigma_\varepsilon \tilde{\varepsilon}^T \hat{\varepsilon}$$
$$= -k_1 s^T s - k_2 s^T \text{sign}(s) + s^T \tilde{\varepsilon} + \sigma_w \tilde{W}^T \hat{W} + \sigma_\varepsilon \tilde{\varepsilon}^T \hat{\varepsilon}$$
$$\le -k_1 \|s\|^2 - k_2 \|s\| + 0.5\|s\|^2 + 0.5\|\tilde{\varepsilon}\|^2 - 0.5\sigma_w \|\tilde{W}\|^2$$
$$\quad + 0.5\sigma_w \|W\|^2 - 0.5\sigma_\varepsilon \|\tilde{\varepsilon}\|^2 + 0.5\sigma_\varepsilon \|\varepsilon\|^2$$
$$\le -(k_1 - 0.5) \|s\|^2 - 0.5 (\sigma_\varepsilon - 1) \|\tilde{\varepsilon}\|^2$$
$$\quad - 0.5\sigma_w \|\tilde{W}\|^2 + 0.5\sigma_w \|W\|^2 + 0.5\sigma_\varepsilon \|\varepsilon\|^2, \quad (34)$$

which can be rewritten as

$$\dot{V}_2 \le -\kappa_c V_2 + \Theta, \quad (35)$$

where $\kappa_c = \min\{(k_1 - 0.5), 0.5(\sigma_\varepsilon - 1), 0.5\sigma_w\}/0.5 * \max\{1, \|\Gamma_s^{-1}\|, \eta^{-1}\}$, $\Theta = 0.5\sigma_w \|W\|^2 + 0.5\sigma_\varepsilon \|\varepsilon\|^2$. To guarantee the closed-loop stability of the investigated system, the parameters should satisfy the following conditions: $k_1 > 0.5$, $k_2 > 0$, $\sigma_\varepsilon > 1$, and $\sigma_\omega > 0$. This will guarantee that κ_c will always have a positive sign, and thus the controlled system states will be bounded. From the above analysis, it can be concluded that s, $\tilde{W}$, and $\tilde{\varepsilon}$ are uniformly ultimately bounded (UUB). The proof is completed.

C. Overall Closed-loop Stability Proof

Once s is converged to zero, $\dot{s}$ will be maintained at zero in the presence of the disturbance, which infers that $u_s = -d$ in the steady status. Therefore, when the system trajectory stays at the sliding mode, the SMC controller u_s can remove the effects of the disturbance. In the proof of the overall stability, u_s can be changed by its equivalent value to facilitate the analysis. Therefore the system stability with the input saturation can be concluded in the following theorem:

Theorem 2: For the given system (22), there exists a scalar $\rho^* > 0$, such that for $|\rho(r, z)| \leq \rho^*$, the developed NN-based ISMC control law u which incorporates (28) and (30) will force the output z to follow the time-varying reference r asymptotically, if the following conditions are satisfied: 1) There exists a scalar $\tau \in (0, 1)$ and $c_\tau > 0$ as the largest scalar such that $\forall \xi \in \boldsymbol{X}(F, c_\tau) = \{\xi \mid \xi^T P \xi \leqslant c_\tau\} \Rightarrow |F\xi| \leqslant (1 - \tau) u_{\max}$, where $\boldsymbol{X}(F, c_\tau)$ is a set of ξ which satisfies the predefined conditions; 2) The initial value $\xi_0 = [\xi_1(0), \xi_2(0), \xi_3(0)]^T$ satisfies $(\xi_0 - \bar{\xi}_0) \in X(F, c_\tau)$; 3) The desired signal, its time-derivative and the disturbance bound satisfy: $|Hr| + |G_r \dot{r}| + d_{\max} \leq \tau u_{\max}$, where $H = G_c + F\bar{G}$.

Proof: Considering (28), the controller u is rewritten as

$$u = F\xi + Hr + G_r \dot{r} + \rho(r, z) B^T P_c \xi_e + u_s. \quad (36)$$

According to the definitions of G_r and $\bar{\xi}$, it is deducted that

$$(A + BF)\bar{\xi} + BG_c r = 0. \quad (37)$$

Then we can transform the closed-loop form of the investigated system (22) into

$$\dot{\xi}_e = (A + BF)\xi_e + B\eta, \quad (38)$$

where η represents

$$\eta = \text{sat}(u) - (F\xi_e + Hr + G_r \dot{r} - d). \quad (39)$$

Given the second and first requirements are satisfied, we have

$$|F\xi_e + Hr + G_r \dot{r} - d| \leq |F\xi_e| + |Hr| + |G_r \dot{r}| + d_{\max} \leq u_{\max}. \quad (40)$$

The value of η can be obtained from (36) according to the input magnitude as

1) If $|u| \leq u_{\max}$, based on $u_s + d = 0$, we have

$$\begin{aligned}\eta &= u - (F\xi_e + Hr + G_r \dot{r} - d) \\ &= \rho(r, z) B^T P_c \xi_e;\end{aligned} \quad (41)$$

2) If $u < -u_{\max}$, therefore,

$$\begin{aligned}\eta &= -u_{\max} - (F\xi_e + Hr + G_r \dot{r} - d) \\ &= -u_{\max} - u + \rho(r, z) B^T P_c \xi_e.\end{aligned} \quad (42)$$

From (40) we can derive that $\rho(r, z) B^T P_c \xi_e < \eta < 0$;

3) If $u > u_{\max}$, therefore,

$$\begin{aligned}\eta &= u_{\max} - (F\xi_e + Hr + G_r \dot{r} - d) \\ &= u_{\max} - u + \rho(r, z) B^T P_c \xi_e.\end{aligned} \quad (43)$$

From (40) it is derived that $0 < \eta < \rho(r, z) B^T P_c \xi_e$.

Considering all the possible cases from (41)-(43), η can be always written as $\eta = q\rho B^T P_c \xi_e$, where $q \in [0, 1]$. If all the conditions are satisfied, the closed-loop system can be transformed into

$$\dot{\xi}_e = (A + BF + q\rho BB^T P_c)\xi_e. \quad (44)$$

A Lyapunov function can be developed as $V_3 = \xi_e^T P_c \xi_e$,

TABLE I
VEHICLE PARAMETERS USED IN THE SIMULATION

Definition and Symbol	Value
Total Vehicle mass m	1500 kg
Vehicle sprung mass m_s	1360 kg
Left/right unsprung mass of the vehicle m_f	35 kg
Left/right tire vertical stiffness k_t	228000 N/m
Left/right suspension stiffness k_s	27000 N/m
Left/right suspension damping coefficient c_p	3000 N/m
Moment of inertia about Z axis I_z	3200 kg·m^2
Moment of inertia about X axis I_x	614 kg·m^2
Wheel track width l_t	1.539 m
Distance between the roll center to the CG of the sprung mass h_r	0.21 m
Distance of CG from front axle l_f	1 m
Distance of CG from rear axle l_r	1.6 m
Cornering stiffness of front tires $c_{f,r}$	78000 N/rad

whose derivative with respect to time can be derived as

$$\begin{aligned}\dot{V}_3 &= -\xi_e^T W_c \xi_e + 2\xi_e^T P_c B\eta \\ &= \xi_e^T \left[-W_c + 2q\rho(B^T P_c)^T B^T P_c\right] \xi_e \leq -\xi_e^T W_c \xi_e.\end{aligned} \quad (45)$$

For any nonpositive function $\rho(r, z)$ which satisfies $|\rho(r, z)| \leq \rho^*$, we can conclude that $\dot{V}_3 < 0$. Since the overall system is proved to be asymptotically stable, it can be concluded that $\lim_{t \to \infty} \xi_e = 0 \Rightarrow \lim_{t \to \infty} \xi(t) = \bar{\xi}$, finally we have $\lim_{t \to \infty} z(t) = C_2 \xi = r$. This completes the proof.

V. SIMULATION RESULTS

In this section, the high-fidelity J-turn and lane-change simulations are implemented on CarSim-Matlab platform, with a nonlinear tire model, which incorporates the uncertainties and disturbances. In the simulation implementation, different road friction conditions and vehicle speeds are adopted. The control desire is to make the vehicle track the reference path with high transient performance. The physical parameters of the vehicle used in the simulation are presented in Table I [42], which are extracted from the CarSim software. The schematic diagram of the high-fidelity CarSim-Matlab platform is shown in Fig. 5, where high-fidelity car model, practical road conditions and driving maneuvers are embedded in CarSim, whose model dynamics and measured states signal then are transferred into Simulink for the state estimation and control verification purpose. The curvatures of the desired paths used in the J-turn and lane-change simulations are respectively shown in Fig. 6.

Considering the physical limitation of the steering actuator and the real implementation, the constraint of the front steering angle is chosen as 0.2 rad. Note that the motivation of choosing this value is to ensure driving safety in the critical scenarios, e.g., slippery road or highway. The observer gains are chosen as $Q = \text{diag}\{1 \times 10^{-2}, 2 \times 10^{-5}, 2 \times 10^{-5}, 1 \times 10^{-4}\}$, $R = \text{diag}\{2 \times 10^{-5}, 1 \times 10^{-5}\}$. The yaw rate reference gains in (2) are chosen as $\ell_1 = 3/v_x$, $\ell_2 = \ell_1 v_x$. For the CNF controller, we have chosen $F = [-3.65, -0.19, -0.096]$, $W_c = \text{diag}\{0.3, 0.08, 0.08\}$, $\alpha = 0.03$, $\phi = 0.05$. The gains of NN compensator are given as $\sigma_\omega = 0.4$, $\sigma_\varepsilon = 1.2$, $\Gamma_s = 0.15$, and $\eta = 0.02$. To validate the superiority of the developed NN-based ISMC technique, we have compared it
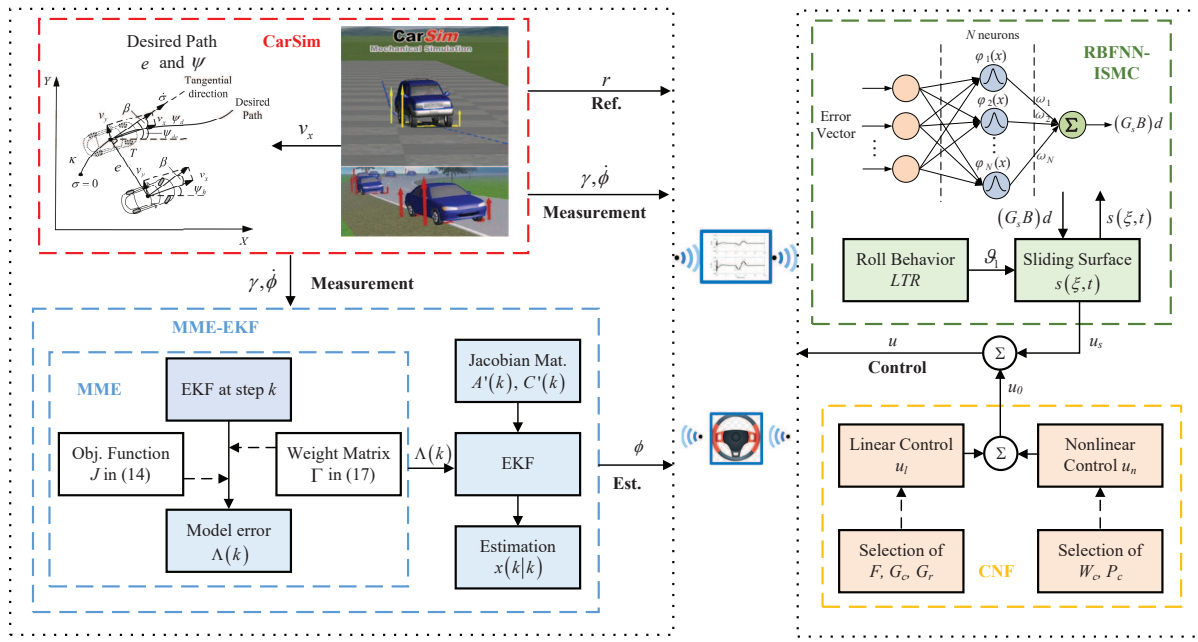
Fig. 5.   Schematic diagram of the high-fidelity CarSim-Matlab platform.
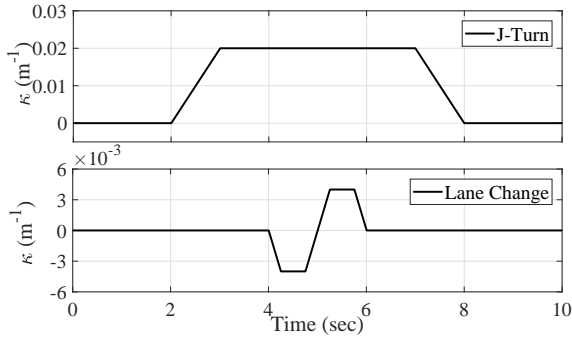

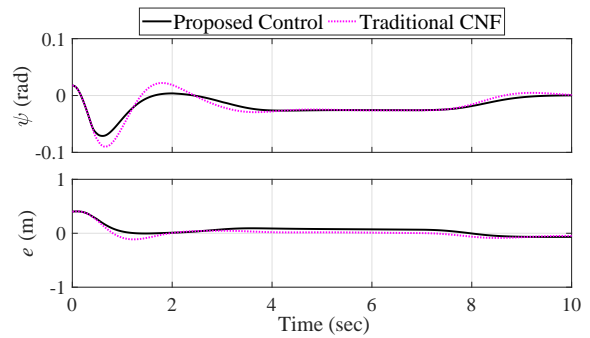Fig. 6.   Curvatures of the desired paths used in the simulations.

Fig. 7.   Heading error and lateral offset results in the J-turn simulation.

with the traditional CNF in [37], where the system disturbance rejection or time variation of the reference was not considered.

Note that the proposed estimator, MME-EKF and controller, ISMC have good robustness to deal with the sensor drift and noise. We have used the CarSim platform to verify the effectiveness of the proposed estimator and controller, where the sensor drift and noise are in reasonably small regions, and have very limited effects on the estimation and control effects, which can be found in the following simulation results.

A. J-Turn Simulation

In the J-Turn simulation, the vehicle runs at a low speed ($v_x = 10$ m/s) on a slippery road with a low tire-road friction coefficient ($\mu = 0.4$, where μ is the tire-road friction coefficient), and is controlled to make a J-turn manoeuver.

The heading error and lateral offset results are plotted in Fig. 7, from which, one can find both the developed controller and traditional CNF can stabilize the path-tracking errors, but the developed control can generate better transient tracking performance. Path-tracking errors have lower overshoots and

faster responses with the developed controller. Note that the lateral offset is stabilized at zero, however, there are still some SSEs in the heading errors. The nonzero heading-error is generally caused by the lateral speed which is kept for a smooth steering when the vehicle runs around a sharp corner. The developed sideslip-angle compensation can reduce the SSEs of the path-tracking errors to a certain extent, which was elaborated in previous literature [13]. Since we suppose the lateral offset is more significant in items of the path-tracking performance and vehicle safety, we have collocated more effort in the lateral-offset control. Considering that the transient path of the lateral offset is enhanced, we can find the developed approach can considerably improve the vehicle security.

The estimation result for the roll angle is shown in Fig. 8. It can be found that the estimation is sufficiently accurate in the whole process, although it is large at the beginning (0-1 second), it is still maintained in a reasonable magnitude, even during 7-8 second when the path curvature rapidly changes. Note that we have used high-fidelity built-in tire model and suspension systems in the simulation study, where the un-
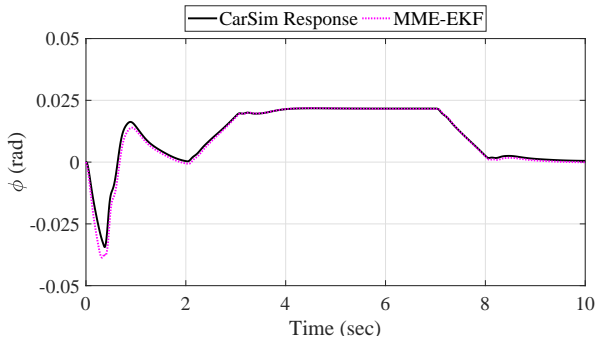
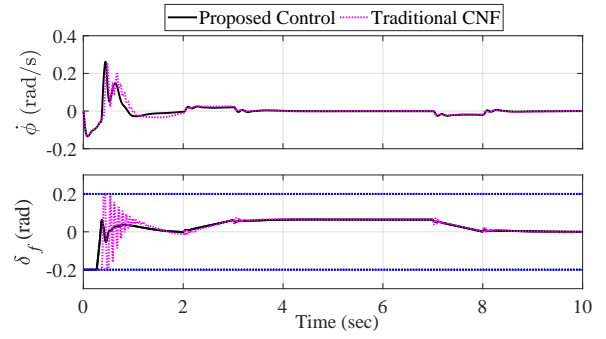Fig. 8.   Roll angle result in the J-turn simulation.

Fig. 10.   Roll rate and steering angle results in the J-turn simulation.
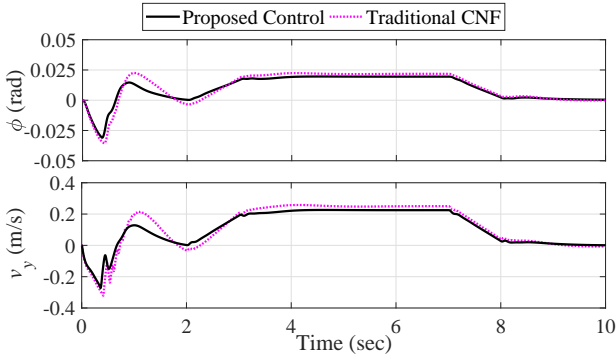

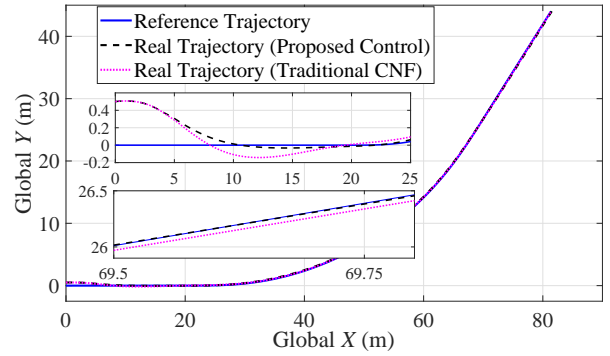Fig. 9.   Roll angle and lateral velocity results in the J-turn simulation.

Fig. 11.   Path-tracking trajectory results in the J-turn simulation.

known system uncertainties are involved. The high accuracy of the roll-angle observation shows the effectiveness of the developed MME-EKF method, which is of great importance in the subsequent feedback control and the overall path-tracking performance. The result of roll angle and lateral velocity are shown in Fig. 9, from which it is found they are both controlled within the reasonable regions, which indicates the vehicle roll and lateral stabilities are maintained, and their transient performances are improved by the proposed control.

The roll rate and steering angle results are shown in Fig. 10. It can be found that the transient performance for the vehicle state and control input have been effectively improved. The roll angle and rate are both maintained in safe regions. The drastic oscillations in the roll rate are caused by the changing path-curvature at the beginning. It is maintained around zero in the steady state by both approaches. For the control input result, one can observe that both methods can maintain the steering input in the prescribed constraint, which is an advantageous characteristic of the CNF algorithm. However, one can apparently find there are drastic shakes in the steering angle result under the traditional CNF control, which is caused by the unknown system uncertainties in the initial phase. Consequentially the vehicle states will also have large oscillations, that may lead to the mechanism wear, or even system instability and insecurity. The smooth input signal is of great significance to guarantee the path-tracking performance, therefore it is implied that the developed control strategy has distinct superiority for yielding high performance for all the system states and inputs.

The global path-tracking trajectory is plotted in Fig. 11,

including the reference trajectory, real trajectories regulated by the developed and the traditional CNF controllers, respectively. We find the developed control can effectively promote the transient tracking performance, including reducing the overshoots, accelerating the convergence speed and reducing the SSEs. With the comparison with the two controllers, it can be concluded that the developed control law can effectively enhance the traditional CNF's ability in improving the transient tracking performance considering multiple control targets, and thus can further guarantee the vehicle stability, safety, and ride comfort with less expensive sensors.

B. Lane-Change Simulation

In the second simulation, the vehicle travels in the highway with a high speed ($v_x = 30$ m/s) on a dry road with a high tire-road friction coefficient ($\mu = 0.8$). Lane change is an indispensable but dangerous manoeuver in highway, which may be more likely to cause lateral slip or rollover. So in this case study, the vehicle is controlled to make a lane change with high speed within about 3 seconds.

The path-following error results in the lane-change simulation are shown in Fig. 12. From this figure we find both path-following errors are converged to zero, under both methods. Note that the steady-state error for the heading error in the lane-change simulation is much smaller compared with that in J-turn simulation shown in Fig. 7. That can be explained by, that in the first case study, the vehicle runs in a very slippery road with a very low speed, but conducts a sharp turning (J-turn), which will result in a larger sideslip angle. This
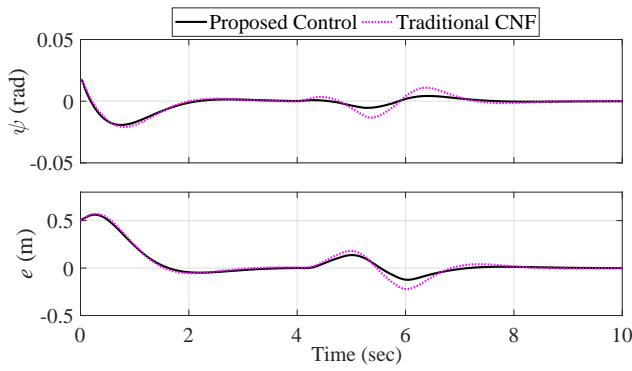
Fig. 12.   Heading error and lateral offset results in the lane-change simulation.
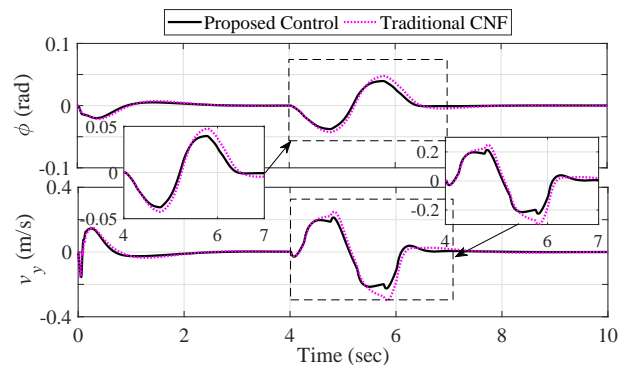

Fig. 14.   Roll angle and lateral velocity results in the lane-change simulation.
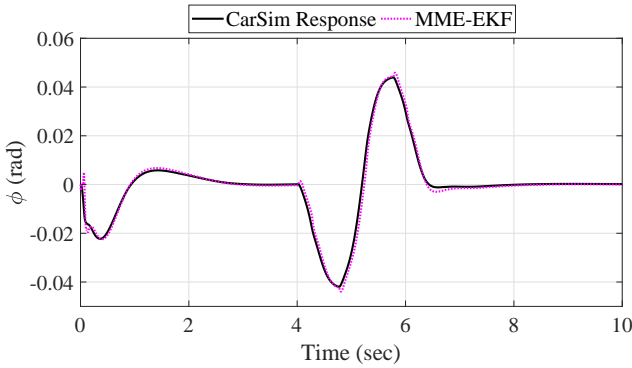

Fig. 13.   Roll angle result in the lane-change simulation.
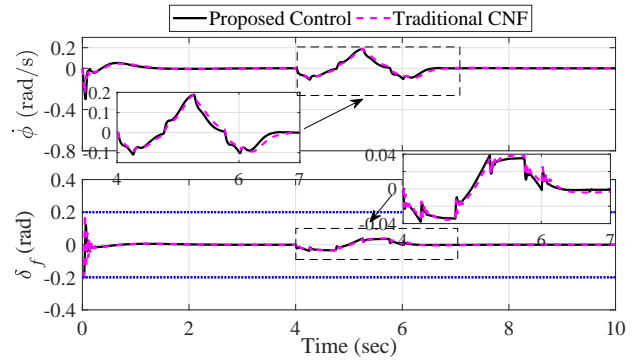

Fig. 15.   Roll rate and steering angle results in the lane-change simulation.

will deteriorate the lateral control and increase the difficulty of converging the heading error. Similarly, we find using the proposed control strategy the path-following errors have smaller overshoots during the lane-change manoeuver, which will further reducing the collision probability.

The estimation result for the roll angle is shown in Fig. 13. From this figure one can see the roll angle estimation is very accurate, with smaller estimation error compared with that in the J-turn simulation. That is because the sideslip angle is smaller when the vehicle travels with high speeds and conducts a small steering angle in lane-changes (which is generally more common and safe) in highways. The results of the roll rate and steering angle input are presented in Fig. 15. Similarly, one can find they are maintained in reasonable regions. As the sideslip angle and steering angle are generally smaller in lane-change manoeuvers, the roll angle and roll rate also have smaller magnitudes compared with J-turns. Both the two methods can maintain the control input within the input constraint, while the proposed controller can effectively reduce the oscillations and lower the overshoots. The roll angle and lateral velocity results in the lane-change simulation are shown in Fig. 14, it is found they are both controlled within the reasonable regions, which indicates the vehicle roll and lateral stabilities are both guaranteed, and their transient responses using the proposed control are better than that using the traditional CNF.

The global path-following trajectory is shown in Fig. 16. From the result of the comparison, we find the proposed control approach is able to yield a more accurate and faster

tracking response, with lower overshoots and steady-state errors, especially in critical driving scenarios, such as when the path curvature severely changes. Till now it is validated that the proposed NN-based control strategy owns better robustness and transient-performance improvement characteristic in different driving conditions and manoeuvers.
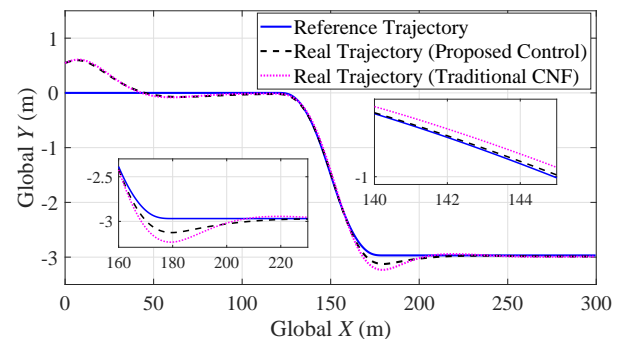

Fig. 16.   Path-following trajectory results in the lane-change simulation.

VI. CONCLUSION

This paper design a robust path-tracking controller with considerations of the system uncertainties, state immeasurabilities, and steering angle constraint. A novel comprehensive ISMC strategy is developed based on the MME-EKF observer, which is used to cancel the effects of the unmodeled dynamics and system uncertainties in estimation. To promote the transient response, CNF is utilized to design the nominal controller.

An adaptive RBFNN algorithm is developed to approximate the unknown vertical vehicle states. The overall stability is rigorously proved using Lyapunov approach. The comparative simulation study with high-fidelity vehicle model based on CarSim-Matlab platform has verified the effectiveness and superiority of the developed control. Limitation of the proposed approach would be we didn't consider the vehicle parameter uncertainties or the variation of the longitudinal speed in the controller design, and we will involve that with other appropriate nonlinear control strategies in our future study.
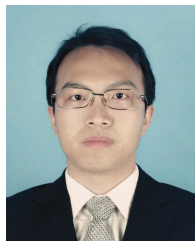
ACKNOWLEDGMENT

REFERENCES

[1] J. Wang, J. Wang, R. Wang, C. Hu, "A framework of vehicle trajectory replanning in lane exchanging with considerations of driver characteristics," *IEEE Trans. Veh. Technol.*, vol. 66, no. 5, pp. 3583-3596, May 2017.

[2] S. H. Kong, and S. Y. Jun, "Cooperative Positioning Technique With Decentralized Malicious Vehicle Detection," *IEEE Trans. Intell. Transp. Syst.*, vol. 19, no. 3, pp. 826-838, Mar. 2018.

[3] H. Cao, S. Zhao, X. Song, S. Bao, M. Li, Z. Huang, and C. Hu, "An optimal hierarchical framework of the trajectory following by convex optimization for highly automated driving vehicles," *Veh. Syst. Dyn.*, pp. 1-31, Jul. 2018.

[4] Y. Lv, X. Zhang, W. Kang, Y. Duan, "Managing emergency traffic evacuation with a partially random destination allocation strategy: A computational-experiment-based optimization approach," *IEEE Trans. Intell. Transport. Syst.*, vol. 16, no. 4, pp. 2182-2191, Aug. 2015.

[5] C. Lv, Y. Liu, X. Hu, H. Guo, D. Cao, and F. Y. Wang, "Simultaneous Observation of Hybrid States for Cyber-Physical Systems: A Case Study of Electric Vehicle Powertrain," *IEEE T. Cybern.*, vol. 48, no. 8, pp. 2357-2367, Aug. 2018.

[6] J. Kim, and D. Kum, "Collision Risk Assessment Algorithm via Lane-Based Probabilistic Motion Prediction of Surrounding Vehicles," *IEEE Trans. Intell. Transp. Syst.*, vol. 19, no. 9, pp. 2965-2976, Sept. 2018.

[7] C. Hu, R. Wang, F. Yan, Y. Huang, H. Wang, and C. Wei, "Differential steering based yaw stabilization using ISMC for independently actuated electric vehicles," *IEEE Trans. Intell. Transp. Syst.*, vol. 19, no. 2, pp. 627-638, Feb. 2018.

[8] J. Han, D. Kum, and Y. Park, "Synthesis of predictive equivalent consumption minimization strategy for hybrid electric vehicles based on closed-form solution of optimal equivalence factor," *IEEE Trans. Veh. Technol.*, vol. 66, no. 7, pp. 5604-5616, Jul. 2017.

[9] J. Na, Y. Huang, X, Wu, G. Gao, G. Herrmann, and J. Z. Jiang, "Active adaptive estimation and control for vehicle suspensions with prescribed performance," *IEEE Trans. Control Syst. Technol.*, vol. 26 , no. 6, pp. 2063-2077, Nov. 2018.

[10] X. Jin, G. Yin, C. Bian, J. Chen, P. Li, N. Chen, "Gain-scheduled Vehicle Handling Stability Control via Integration of Active Front Steering and Suspension Systems", *ASME Trans. J. Dyn. Syst. Meas. Control*, vol. 138, no. 1, pp. 014501-1-12, Jan. 2016.

[11] J. Zhao, P. Wong, X. Ma, C. Zheng, "Chassis integrated control for active suspension active front steering and direct yaw moment systems using hierarchical strategy", *Veh. Syst. Dyn.*, vol. 55, no. 1, pp. 72-103, Jan. 2017.

[12] Y. Qin, C. Wei, X. Tang, N. Zhang, M. Dong, and C. Hu, "A novel nonlinear road profile classification approach for controllable suspension system: Simulation and experimental validation," *Mech. Syst. Signal Proc.*, vol. 125, pp. 79-98, 15 Jun. 2019.

[13] C. Hu, R. Wang, F. Yan, and N. Chen, "Should the desired heading in path following of autonomous vehicles be the tangent direction of the desired path?" *IEEE Trans. Intell. Transp. Syst.*, vol. 16. no. 6, pp. 3084-3094, Dec. 2015.

[14] J. Guo, Y. Luo, K. Li, "An Adaptive Hierarchical Trajectory Following Control Approach of Autonomous Four-Wheel Independent Drive Electric Vehicles," *IEEE Trans. Intell. Transp. Syst.*, vol. 19, no. 8, pp. 2482-2492, Aug. 2018.

[15] W. Kim, Y. S. Son, and C. C. Chung, "Torque-overlay-based robust steering wheel angle control of electrical power steering for a lane-keeping system of automated vehicles," *IEEE Trans. Veh. Technol.*, vol. 65, no. 6, pp. 4379-4392, Jun. 2016.

[16] H. Jing, R. Wang, J. Wang, N. Chen, "Robust H_∞ dynamic output-feedback control for four-wheel independently actuated electric ground vehicles through integrated AFS/DYC," *J. Frankl. Inst.*, vol. 355, no. 18, pp. 9321-9350, Dec. 2018.

[17] J. Ackermann, *Robust Control: The Parameter Space Approach*, New York, NY, USA:Springer-Verlag, 2002.

[18] Y. Huang, J. Na, X. Wu, and G. Gao, "Approximation-free control for vehicle active suspensions with hydraulic actuator," *IEEE Trans. Ind. Electron.*, vol. 65, no. 9, pp. 7258-7267, Sep. 2018.

[19] K. Nam, S. Oh, H. Fujimoto, and Y. Hori, "Estimation of sideslip and roll angles of electric vehicles using lateral tire force sensors through RLS and Kalman filter approaches," *IEEE Trans. Ind. Electron.*, vol. 60, no. 3, pp. 988-1000, Mar. 2013.

[20] G. Jia, L. Li, and D. Cao, "Model-based estimation for vehicle dynamics states at the limit handling," *J. Dyn. Syst. Meas. Control*, vol. 137, no. 10, pp. 1-8, Oct. 2015.

[21] C. Hu, R. Wang, F. Yan, and N. Chen, "Output constraint control on path following of four-wheel independently actuated autonomous ground vehicles," *IEEE Trans. Veh. Technol.*, vol. 65, no. 6, pp. 4033-4043, Jun. 2016.

[22] K. Kritayakirana, and J. C.Gerdes, "Using the centre of percussion to design a steering controller for an autonomous race car," *Veh. Syst. Dyn.*, vol. 50, sup. 1, pp. 33-51, Jul. 2012.

[23] H. Imine, and M. Djemai, "Switched Control for Reducing Impact of Vertical Forces on Road and Heavy-Vehicle Rollover Avoidance," *IEEE Trans. Veh. Technol.*, vol. 65, no. 6, pp. 4044-4052, Jun. 2016.

[24] Y. Qin, Z. Wang, C. Xiang, E. Hashemi, A. Khajepour, and Y. Huang, "Speed independent road classification strategy based on vehicle response: Theory and experimental validation," *Mech. Syst. Signal Proc.*, vol. 117, pp. 653-666, Feb. 2019.

[25] G. P. Rajamani and Rajesh, "Real-time estimation of rollover index for tripped rolloverswith a novel unknown input nonlinear observer," *IEEE-ASME Trans. Mechatron.*, vol. 19, no. 2, pp. 743-754, Apr. 2014.

[26] Z. Wang, Y. Qin, C. Hu, M. Dong, and Fei Li, "Fuzzy Observer-based Prescribed Performance Control of Vehicle Roll Behavior via Controllable Damper," *IEEE Access*, vol. 7, pp. 19471-19487, Jan. 2019.

[27] W. Liu, H. He, and F. Sun, "Vehicle state estimation based on minimum model error criterion combining with extended kalman filter," *J. Frankl. Inst.*, vol. 353, no. 4, pp. 834–856, Mar. 2016.

[28] C. Hu, R. Wang, and F. Yan, "Integral sliding mode-based composite nonlinear feedback control for path following of four-wheel independently actuated autonomous vehicles," *IEEE Trans. Transport. Electrification*, vol. 2, no. 2, pp. 221-230, Jun. 2016.

[29] I. C. Baik, K. H. Kim, M. J. Youn, "Robust nonlinear speed control of PM synchronous motor using boundary layer integral sliding mode control technique," *IEEE Trans. Control Syst. Technol.*, vol. 8, no. 1, pp. 47-54, Jan. 2000.

[30] M. Rubagotti, A. Estrada, F. Castanos, A. Ferrara, L. Fridman, "Integral sliding mode control for nonlinear systems with matched and unmatched perturbations," *IEEE Trans. Autom. Control*, vol. 56, no. 11, pp. 2699-2704, Nov. 2011.

[31] R. Rajamani, and D. N. Piyabongkarn, "New paradigms for the integration of yaw stability and rollover prevention functions in vehicle stability control," *IEEE Trans. Intell. Transp. Syst.*, vol. 14, no. 1, pp. 249-261, Mar. 2013.

[32] J. Yang, S. Li, X. Yu, "Sliding-mode control for systems with mismatched uncertainties via a disturbance observer," *IEEE Trans. Ind. Electron.*, vol. 60, pp. 160-169, Jan. 2013.

[33] E. Kayacan, "Sliding mode control for systems with mismatched time-varying uncertainties via a self-learning disturbance observer," *Trans. Inst. Meas. Control*, 0142331218794266, Sep. 2018.

[34] C. L. P. Chen, G.-X. Wen, Y.-J. Liu, and Z. Liu, "Observer-based adaptive backstepping consensus tracking control for high-order nonlinear semi-strict-feedback multiagent systems," *IEEE Trans. Cybern.*, vol. 46, no. 7, pp. 1591-1601, Jul. 2016.

[35] W. He, Z. Yan, C. Sun, Y. Chen, "Adaptive neural network control of a flapping wing micro aerial vehicle with disturbance observer," *IEEE Trans. Cybern.*, vol. 47, no. 10, pp. 3452-3465, Oct. 2017.

[36] S. S. Ge, C. C. Hang, H. T. Lee, T. Zhang, *Stable Adaptive Neural Network Control*, New York, NY, USA:Springer-Verlag, 2002.

[37] W. Lan, C. K. Thum and B. M. Chen, "A hard disk drive servo system design using composite nonlinear feedback control with optimal nonlinear gain tuning methods," *IEEE Trans. Ind. Electron.*, vol. 57, no. 5, pp.1735-1745, May 2010.

[38] L. Zhang, K. Li, and E. W. Bai, "A new extension of newton algorithm for nonlinear system modeling using RBF neural networks," *IEEE Trans. Autom. Control*, vol. 58, no. 11, pp. 2929-2933, Nov. 2013.

[39] Y. Qin, Z. Wang, C. Xiang, M. Dong, C. Hu, R. Wang, "A Novel Global Sensitivity Analysis on the Observation Accuracy of the Coupled Vehicle Model," *Veh. Syst. Dyn.*, pp.1-22., Sep. 2018.

[40] G. Chowdhary, E. N. Johnson, "Theory and flight-test validation of a concurrent-learning adaptive controller," *AIAA J. Guid. Control Dyn.*, vol. 34, pp. 592-607, 2010.

[41] G. Chowdhary and E. Johnson, "Concurrent learning for convergence in adaptive control without persistency of excitation," in *Proc. 49th IEEE Conf. Decision and Control*, Dec. 2010, pp. 3674-3679.

[42] Z. Wang, Y. Qin, L. Gu, and M. Dong, "Vehicle System State Estimation Based on Adaptive Unscented Kalman Filtering Combing With Road Classification," *IEEE Access*, vol. 5, pp. 27786-27799, Nov. 2017.

Jing Na (M' 15) received the B.Eng. and Ph.D. degrees in control engineering from the School of Automation, Beijing Institute of Technology, Beijing, China, in 2004 and 2010, respectively. From 2011 to 2013, he was a Monaco/ITER Post-Doctoral Fellow with ITER Organization, Saint-Paul-lès-Durance, France. From 2015 to 2017, he was a Marie Curie Intra-European Fellow with the Department of Mechanical Engineering, University of Bristol, Bristol, U.K. Since 2010, he has been with the Faculty of Mechanical and Electrical Engineering, Kunming University of Science and Technology, Kunming, China, where he became a Full Professor in 2013. He has co-authored one monograph published in Elsevier and authored or co-authored over 100 international journal and conference papers. His current research interests include intelligent control, adaptive parameter estimation, nonlinear control and applications for robotics, vehicle systems, and wave energy convertor. Dr. Na was a recipient of the Marie Curie Fellowship from EU, the Best Application Paper Award of the 3rd IFAC International Conference on Intelligent Control and Automation Science in 2013, and the 2017 Hsue-Shen Tsien Paper Award. He is currently an Associate Editor of Neurocomputing and has served as the IPC Chair of ICMIC in 2017.

Chuan Hu is currently a Postdoctoral Fellow in the Department of Mechanical Engineering, University of Texas at Austin, Austin, USA. He was a Postdoctoral Fellow in the Department of Systems Design Engineering, University of Waterloo, Waterloo, Canada from July 2017 to July 2018. He received the B.E. degree in vehicle engineering from Tsinghua University, Beijing, China, in 2010, the M.E. degree in vehicle operation engineering from the China Academy of Railway Sciences, Beijing, in 2013, and the Ph.D. degree in Mechanical Engineering, McMaster University, Hamilton, Canada in 2017. His research interest includes vehicle system dynamics and control, motion control and estimation of autonomous vehicles, mechatronics, robust and adaptive control.

Yechen Qin (S' 14-M' 17) received the B.E. degree and Ph.D. degree in mechanical engineering from the Beijing Institute of Technology, China, in 2010 and 2016, respectively, where he currently holds a Postdoctoral position. From 2013 to 2014, he was a Visiting Ph.D. Student with Texas A&M University, USA. From 2017 to 2018, he was a Visiting Scholar with the University of Waterloo. His research interests include controllable suspension systems, road estimation, and in-wheel motor vibration control.

Zhenfeng Wang received the M.S. degree from Tsinghua University, Beijing, China, in 2012, and the Ph.D. degree in mechanical engineering from the Beijing Institute of Technology, China, in 2018. From 2017 to 2018, he was a Visiting Scholar with the University of Waterloo. He is working on the vehicle dynamics, state estimation, and modeling for vehicle and suspension systems. His research interests include vehicle dynamics and control, nonlinear state estimation, and controllable suspension systems.

Jinghua Guo received the Ph.D. degrees from Dalian University of Technology, China, in 2012. From 2012 to 2015, he finished his postdoctoral research in Tsinghua University. He is currently an associate professor with Xiamen University. He has authored more than 30 journal papers. He has engaged in more than five sponsored projects. His current research interests include intelligent vehicles, vision system, control theory and applications.

Hamid Taghavifar (M' 18) is currently a Horizon Postdoctoral Fellow at Department of Mechanical, Industrial and Aerospace Engineering, CONCAVE Research Center, Concordia University, Canada. He received his Ph.D. in Mechanical Engineering from Urmia University, Iran, in 2016. His research focuses on vehicle dynamics and control, adaptive and nonlinear controls, artificial intelligence, and optimizations, where he has contributed over 45 papers, a book and 2 Iranian registered patents. He serves as the Editor-inChief of Journal of Advances in Vehicle Engineering, Editor for Int. J. of Vehicle Systems Modelling and Testing and Int. J. of Vehicle Information and Communication Systems.

Chongfeng Wei obtained the B.Sc. degree in computational and applied mathematics and the M.Sc. degree in vehicle engineering from Southwest Jiaotong University, Chendu, China, in 2009 and 2011, respectively, and the Ph.D. degree in mechanical engineering from the University of Birmingham in 2015. After two and a half years postdoctoral research period, he joined the School of Mechanical Engineering at Shanghai Jiao Tong University as an Assistant Professor (tenure-track). He then moved to the institute of Transport Studies at University of Leeds as a research fellow in 2018. His current research focuses on Humanlike autonomous vehicle control and collision avoidance.